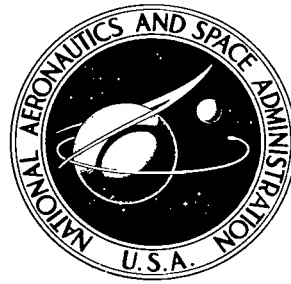


NASA TECHNICAL NOTE



NASA TN D-6341

2.1

NASA TN D-6341

LOAN COPY: RETURN  
AFWL (DOGL)  
KIRTLAND AFB, N.



A STUDY OF THE FEASIBILITY  
OF APPLYING CAPACITIVE  
DISPLACEMENT-MEASURING TECHNIQUES  
TO OPEN-MESH GRID STRUCTURES

*by Richard DeLoach*  
*Langley Research Center*  
*Hampton, Va. 23365*





0132873

1. Report No. NASA TN D-6341	2. Government Accession No.	3. Recipien 0132873
4. Title and Subtitle A STUDY OF THE FEASIBILITY OF APPLYING CAPACITIVE DISPLACEMENT-MEASURING TECHNIQUES TO OPEN-MESH GRID STRUCTURES		5. Report Date September 1971
7. Author(s) Richard DeLoach		6. Performing Organization Code
9. Performing Organization Name and Address NASA Langley Research Center Hampton, Va. 23365		8. Performing Organization Report No. L-7465
12. Sponsoring Agency Name and Address National Aeronautics and Space Administration Washington, D.C. 20546		10. Work Unit No. 134-14-06-05
15. Supplementary Notes Appendix A by Norman C. Wenger, Lewis Research Center		11. Contract or Grant No.
16. Abstract <p>This paper provides theoretical and experimental support for the hypothesis that a noncontacting capacitive displacement-measuring transducer can be used to measure displacements in structures with extremely small surface areas. Examples of such structures include reflector nets which form the primary substructures of radio telescopes and radar receiving units. Test models of this kind of structure are typically so lightweight and flexible that mounted transducers would alter their natural response to input test moments and forces. Noncontacting transducers are therefore required for modal analysis and structural stability tests on this class of structure.</p> <p>This paper evaluates the feasibility of employing a capacitive probe in displacement measurements of structures with low surface areas, particularly open-mesh grid structures. The field of a square-mesh grid-plate capacitor is solved. A variational technique is used to determine the capacitance of the grid-plate capacitor in terms of easily measured geometric parameters. The derived theoretical capacitance formula predicts grid-plate capacitance values which are orders of magnitude larger than preliminary intuitive estimations. The theory is supported with experimental data. A laboratory prototype system is described which is capable of resolving displacements on the order of 0.01 mm in a 15-cm-square open-mesh grid with the probe as far away from the net as 25 cm.</p>	13. Type of Report and Period Covered Technical Note	
17. Key Words (Suggested by Author(s)) Capacitive probe Open-mesh grid Displacement measurement	18. Distribution Statement Unclassified - Unlimited	14. Sponsoring Agency Code
19. Security Classif. (of this report) Unclassified	20. Security Classif. (of this page) Unclassified	21. No. of Pages 42
		22. Price* \$3.00

A STUDY OF THE FEASIBILITY OF APPLYING CAPACITIVE  
DISPLACEMENT-MEASURING TECHNIQUES TO  
OPEN-MESH GRID STRUCTURES

By Richard DeLoach  
Langley Research Center

SUMMARY

This paper provides theoretical and experimental support for the hypothesis that a noncontacting capacitive displacement-measuring transducer can be used to measure displacements in open-mesh grid structures with extremely small surface areas. Examples of such structures include reflector nets which form the primary substructures of radio telescopes and radar receiving units. Test models of this kind of structure are typically so lightweight and flexible that mounted transducers would alter their dynamic response characteristics. Noncontacting transducers are therefore required for modal analysis and structural stability tests on this class of structure.

The purpose of the paper is to evaluate the feasibility of employing a capacitive probe in displacement measurements of structures with low surface areas, particularly open-mesh grid structures. A solution is found for the field of a charged square-mesh grid mounted parallel to a flat grounded plate. A variational technique is used to determine the capacitance of this grid-plate capacitor in terms of easily measured geometric parameters. It is known that the capacitance of a parallel-plate capacitor is directly proportional to the area of the plates. Because the relative surface area of a large-mesh grid is extremely small, original estimates of the capacitance of a grid-plate system were correspondingly small. However, the theoretical capacitance formula derived herein predicts grid-plate capacitance values which are orders of magnitude larger than these preliminary estimates. The theory is supported with experimental data. Results show that a noncontacting capacitive transducer is indeed feasible for detecting displacements in surfaces with extremely small surface areas.

INTRODUCTION

The purpose of this report is to demonstrate that a noncontacting capacitive displacement-measuring transducer can be used to measure displacement amplitudes in open-mesh grid structures possessing minute surface areas. Examples of such

structures include the reflector nets which form the primary substructures of radio telescopes and radar receiving units.

In July 1969 a need arose at the Langley Research Center for an instrument to measure the dynamic response of two models of a radio telescope satellite called LOFT (Low Frequency Telescope). Both models have essentially the same overall configuration, which consists of a spin-stabilized reflector net fabricated from an open-mesh grid of flexible, very lightweight strands of rubber-coated steel yarn. The larger model has a diameter of 15 meters while the smaller model has a diameter of 5 meters. The proposed testing program calls for the models to be rapidly rotated in a large vacuum chamber with the resulting centrifugal force used to deploy the reflector net and maintain its shape. (It is necessary to conduct the tests under vacuum to avoid the problems of air drag in deploying the model.) Bursts of forced air from jets mounted on independently rotating exciter arms under the reflector net will be used to excite resonance modes in the net. It is these mode shapes which are to be measured. The tests are complicated by a number of factors. Among the most serious complications are the very small surface area of the reflector net and the fact that it is extremely flexible and lightweight. Conventional mounted transducers are not practical since even the smallest ones available are massive enough to alter the dynamic response of the structure.

It has been suggested that a small, flat plate might be mounted near the reflector so that the reflector net and plate will form a capacitor. As the grid-plate geometry changes as a result of the modal displacements of the net, the grid-plate capacitance will also vary, and these changes in capacitance can be related to the motions of the grid.

Capacitive probes have been in use since 1920 when R. Whiddington and his collaborators first investigated their potential application to the measurement of pressure, temperature, and force, as well as displacement (refs. 1 to 4). Since then, capacitive probes have found an ever-increasing range of applications (ref. 5). However, most of the standard capacitive measurement systems in use today involve very close proximity between the probe and the subject surface (refs. 6 and 7). This close proximity causes a maximum percentage change in capacitance for a given small displacement in the subject surface, providing a high degree of resolution in the measurement system. In the LOFT application, however, close proximity between probe and subject is not practical. Displacement amplitudes on the order of 5 to 10 cm are expected in the tests, which means that the probe must be mounted at least that far from the subject. Actually, in order to avoid fouling the net during model deployment, the probes should be at least 25 cm from the surface of the net. Most capacitive displacement-measuring systems involve probe-subject separations on the order of millimeters or less. Not only are the probe-subject separations necessarily large in the LOFT application, but the relative surface area of the steel yarn which makes up the net is minute. (Each strand is only 0.25 mm in

diameter, while adjacent strands can be on the order of 150 mm apart.) For a given probe, the probe-subject capacitance is proportional to the area of the subject and inversely proportional to the probe-subject separation. Because of the large probe-subject separations and minute subject surface area involved in the test, it was originally feared that the available probe-subject capacitances would be much too small to be practical. It was therefore necessary to determine analytically how the grid-plate capacitance would depend on grid-plate geometry parameters in order to evaluate the feasibility of employing a capacitive transducer in the LOFT tests.

A square-mesh parallel grid-plate capacitor is used as a model for the analysis. The field of such a capacitor is solved, and a variational technique is used to determine the capacitance of the grid-plate capacitor model from the field solution. The theoretical results are compared with experimental data.

### SYMBOLS

$A_n$	capacitance geometry constant, $D_n/V$
$a$	mesh parameter, distance between adjacent parallel wires in grid
$a_n$	general Fourier coefficient
$b$	grid-plate separation
$C$	capacitance
$C_l$	capacitance per unit length of a parallel wire-plate capacitor
$D_n$	potential distribution constant
$d_n$	radial distance from an arbitrary point in the plane of a grid of parallel charged wires to the axis of charge of the $n$ th wire
$d_n'$	radial distance from an arbitrary point in the plane of a grid of parallel charged wires to the axis of charge of the $n$ th image wire
$L$	length of a rectangular parallel-surface capacitor
$n$	positive integer

$q$	excess charge
$r$	wire radius
$T = \frac{\lambda}{8\pi\epsilon V}$	
$U$	electric field energy
$V$	potential difference
$W$	width of a rectangular parallel-surface capacitor
$x,y,z$	Cartesian space coordinates
$\alpha$	separation-of-variables constant
$\delta$	displacement of the axis of charge of a charged wire due to the influence of an adjacent grounded plane (see fig. 4)
$\epsilon$	electric permittivity
$\lambda$	linear charge density
$\tau$	volume of integration
$\phi$	potential distribution

#### ANALYSIS

Figure 1 is a sketch of the grid-plate capacitor which is used as a model for the analysis. The grid is a square mesh of cylindrical wires, each of radius  $r$ , separated axis-to-axis by a distance  $a$ . The grid is parallel to the plate and is separated from it by a distance  $b$ . The grid and the plate have the same length  $L$  and the same width  $W$ . In the analysis, the field of this grid-plate capacitor is solved and a variational technique is used to determine the capacitance from the field solution. This variational technique is described in the following section.

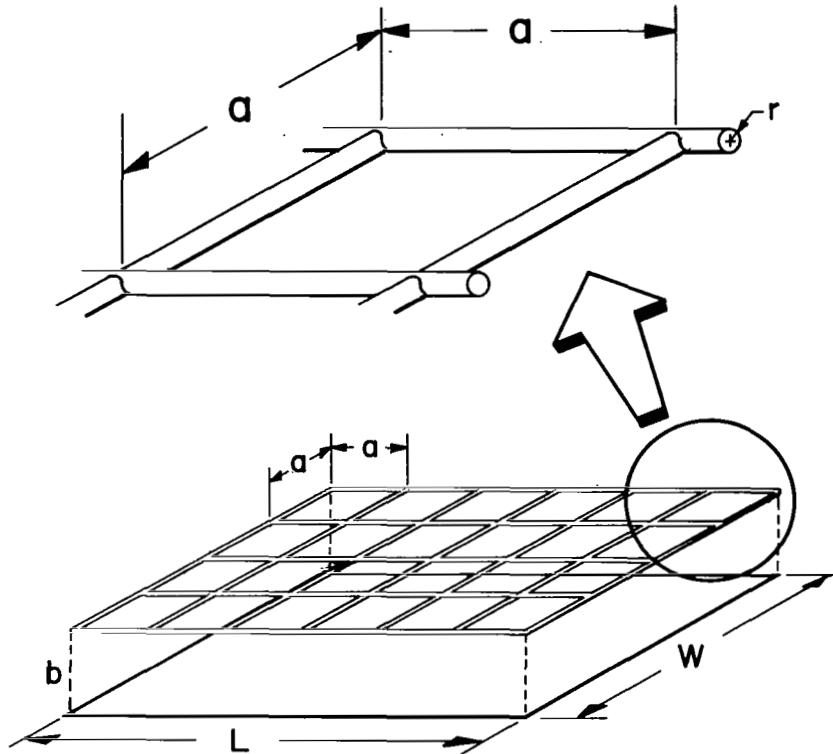


Figure 1.- Parallel grid-plate capacitor.

### Approach

To invoke basic definitions in determining the capacitance of a pair of arbitrary conductors held at some fixed potential difference, it must be possible to determine the total excess charge residing on either of the conductors. For systems possessing relatively complex geometries, this can be a rather difficult task. However, there do exist a number of techniques for determining the potential distribution associated with a charged system. It would therefore be useful to be able to express the capacitance of some arbitrary charged system in terms of the potential distribution of that system. This can be done by equating the energy stored in the field of an arbitrary capacitor to the energy of an arbitrary electric field. If  $U$  is the field energy,  $C$  the capacitance,  $V$  the potential difference, and  $\phi$  the potential distribution between two conductors, the following relation is true in general:

$$U = \frac{1}{2} CV^2 = \frac{\epsilon}{2} \int_{\tau} (\nabla\phi)^2 d\tau \quad (1)$$

The right-hand term describes the energy of an arbitrary electric field bounded by the limits of the volume integral and the middle term describes the energy stored in the

field of an arbitrary charged capacitor, independent of its geometry. It is understood that the volume integral is taken throughout the region bounded by the conductors. The symbol  $\epsilon$  represents the permittivity of the environment (air, vacuum, etc.). It is the product of the permittivity of free space and the dielectric constant of the medium between the conductors. Equation (1) yields the following:

$$C = \frac{\epsilon}{V^2} \int_{\tau} (\nabla\phi)^2 d\tau \quad (2)$$

Thus, the capacitance of an arbitrary condenser charged to a potential difference of  $V$  volts can be expressed in terms of the potential distribution which exists in the region bounded by the plates of the condenser. It is necessary only to find the potential distribution in the region bounded by the condenser when it is charged. But equation (2) also possesses a very remarkable property. Note that it expresses capacitance  $C$  as a function of potential distribution  $\phi$ . Any  $\phi$  can be inserted in equation (2) to generate an expression for capacitance, but obviously only the true  $\phi$  will yield the right capacitance. Of all the possible potential distributions which might exist within a given charged condenser, the question is, which potential distribution  $\phi$  is actually present?

From arguments based on the law of the conservation of energy it can be shown that if two arbitrary fixed conductors are held at a given potential difference, charges will tend to distribute themselves on the surface of the conductors in such a way as to store the least amount of energy in the field between them. This is a special case of Thomson's theorem (ref. 8). From equation (1) it can be seen that the energy stored in a charged condenser is directly proportional to the capacitance of that condenser. It is therefore clear that when a fixed potential difference is impressed between two conductors (a condenser) the charges tend to distribute themselves on the conductors in such a way as to create a potential distribution corresponding to some minimum capacitance. That is, of all the physically realizable values of  $\phi$  that might be used in equation (2), the correct  $\phi$  is the one that generates the smallest value for  $C$ . This is quite significant! According to the ordinary calculus of extremums, if a continuous function has a minimum, then first-order departures from that minimum in the independent variable correspond to departures from the minimum in the dependent variable which are only second order to the deviations of the independent variable. For example, consider some continuous function  $C(\phi)$  which has a minimum at  $\phi_c$ . Then  $C(\phi_c)$  is the minimum of that function. Now consider a first-order departure from  $\phi_c$  in  $\phi$ ; that is, consider  $C(\phi_c + \delta\phi)$ , where  $\delta\phi$  is some first-order departure from  $\phi_c$ . From laws developed in the calculus of extremums it can be shown that  $C(\phi_c + \delta\phi)$  differs from  $C(\phi_c)$  only to second order, even when  $\delta\phi$  is a first-order deviation from  $\phi_c$  (ref. 9). Therefore, if a first-order approximation to  $\phi$  is inserted in equation (2) instead of the true

expression for  $\phi$ , the resulting expression for the capacitance will be a second-order approximation to the correct capacitance because, as was determined above, the true potential distribution  $\phi$  corresponds to a minimum capacitance  $C$ .

The preceding analysis has been based in part on arguments developed in the ordinary calculus of extremums. But  $\phi$  in equation (2) does not represent a variable in the ordinary sense; it represents potential distribution, which is itself a function of coordinate space. It might therefore be argued that an analysis based on the ordinary calculus of extremums does not necessarily apply to equation (2). But the analysis can be rigorously extended to cover the case at hand by invoking the calculus of variations instead of the calculus of extremums. This analysis is a bit more involved than the one that has been outlined and will not be presented here, but the results are the same as if  $\phi$  were treated as an ordinary variable instead of a function (ref. 10).

The important point is that the capacitance of a condenser with a completely arbitrary geometry can be determined from a knowledge of the potential distribution which exists when the condenser is charged to some fixed potential difference. Furthermore, if the true potential distribution is unknown, a second-order approximation to the capacitance can be derived by using only a first-order approximation to the true potential distribution.

As a simple example of an application of this analysis, consider the case of a parallel-plate capacitor with one plate grounded and the other at a potential  $V$  with respect to ground. The grounded plate is assumed to be in the  $z = 0$  plane and the charged plate is in the  $z = b$  plane. The potential distribution, known to be linear, might look like the following:

$$\phi = \frac{Vz}{b} \tag{3}$$

If the plates are rectangular, with length  $L$  and width  $W$ , equation (2) becomes

$$C = \frac{\epsilon}{V^2} \int_{z=0}^{z=b} \int_{y=0}^{y=W} \int_{x=0}^{x=L} \frac{V^2}{b^2} dx dy dz \tag{4}$$

or

$$C = \frac{\epsilon LW}{b} \tag{5}$$

This is recognized as the correct formula for the capacitance of a parallel-plate capacitor with plate dimensions  $L$  by  $W$  separated by a distance  $b$ .

Now the potential will be assumed to be unknown and the capacitance of a parallel-plate condenser will be estimated by inserting a trial potential into equation (2). Of

course, the potential distribution of a parallel-plate capacitor is known to be linear, but to illustrate the usefulness of equation (2) in deriving close approximations to capacitance from rough approximations of potential, a nonlinear potential is inserted into equation (2). Assume, for example, that  $\phi$  is a sinusoidal potential:

$$\phi = V \sin \frac{\pi z}{2b} \quad (6)$$

This potential meets the prescribed boundary conditions but is certainly not linear. To see what sort of capacitance it produces, equation (6) is inserted into equation (2) to yield

$$C = \frac{\epsilon}{V^2} \int_{z=0}^{z=b} \int_{y=0}^{y=W} \int_{x=0}^{x=L} \frac{V^2 \pi^2}{4b^2} \cos^2 \frac{\pi z}{2b} dx dy dz$$

or

$$C = \frac{\pi^2}{8} \frac{\epsilon L W}{b}$$

Note that the sinusoidal trial potential leads to the correct capacitance formula multiplied by a factor slightly greater than 1, namely  $\pi^2/8$ . This is certainly a very close approximation to the true capacitance, considering how poor the potential approximation was. If other incorrect trial functions are used in equation (2), other approximate capacitance formulas will be generated, but just as in this example, the approximation to the correct capacitance will always be much closer to the true capacitance than the trial potential is to the real potential. Actually, a very accurate expression for capacitance can be obtained from a close approximation of the potential; the better the potential approximation, the better the expression for capacitance. This method of deriving second-order approximations to capacitance from first-order approximations to potential is an application of what is called the electrostatic theory of least action. It is a technique whereby approximate solutions can be found to otherwise intractable problems.

In the following sections of this paper, the potential distribution of a grid-plate condenser is determined and used in equation (2) to generate an expression for the capacitance of a grid-plate condenser. The field solution entails a few approximations and therefore is not an exact solution, but because of the variational technique used, the resultant capacitance formula is quite accurate.

#### Two-Dimensional Grid-Plate Potential Distribution

The field problem has been cast in a Cartesian coordinate system with the flat plate (dimensions  $L$  by  $W$ ) in the  $z = 0$  plane and the grid of wires in the  $z = b$  plane. The wires have a radius  $r$  and are separated a distance  $a$  from axis to axis. The

plate is assumed to be grounded (i.e., at 0 potential) and the wires of the grid are at potential  $V$  with respect to the plate. In order to simplify the field problem, the grid is imagined to consist of two "subgrids," one subgrid being composed of wires running parallel to the X-axis and the other being composed of wires running parallel to the Y-axis. The problem is thus simplified into a pair of two-dimensional field problems. The solutions to these two problems are combined to yield the potential distribution of the three-dimensional grid-plate configuration. Figure 2 illustrates one of the subgrids.

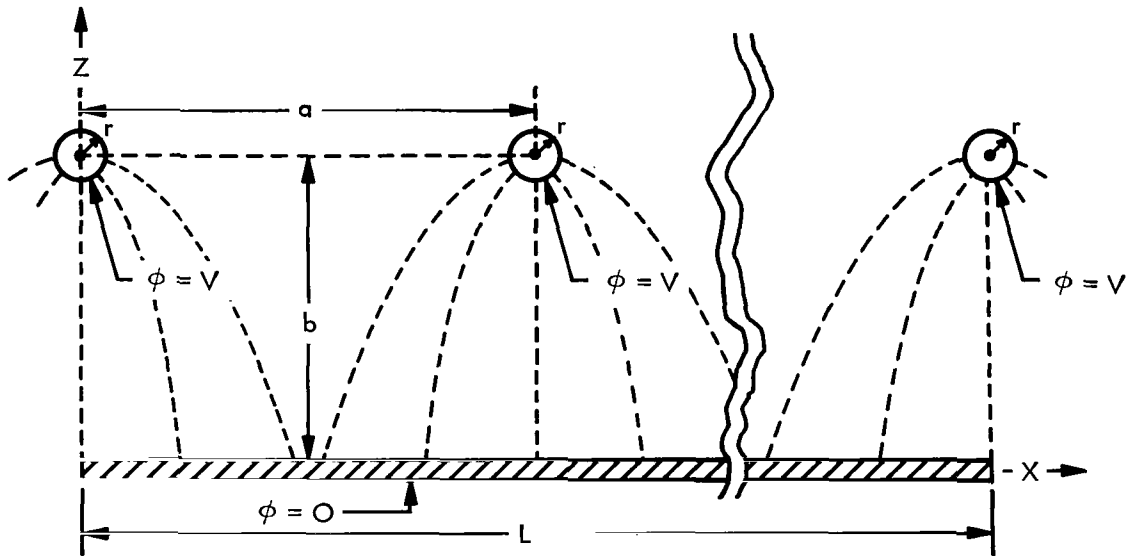


Figure 2.- Field of a grid-plate capacitor.

The potential distribution corresponding to figure 2 must satisfy Laplace's equation and meet the boundary conditions. The uniqueness theorem guarantees that any such solution will be correct and unique.

Laplace's equation in two dimensions, expressed in Cartesian coordinates, is

$$\nabla^2 \phi(x,y) = 0 \tag{7}$$

One possible solution to this equation is

$$\phi = D \cos \alpha x \sinh \alpha z \tag{8}$$

The constants  $D$  and  $\alpha$  must be evaluated to make equation (8) meet the boundary conditions.

Since the wires are indistinguishable,  $\phi$  is the same at  $x = 0$  as at  $x = a$  for any given  $z$ . Then

$$\cos 0 = \cos \alpha a$$

$$\alpha a = 2n\pi \quad (n = 0, 1, 2, 3, \dots)$$

$$\alpha = \frac{2n\pi}{a} \quad (9)$$

$$\phi = D \cos \frac{2n\pi x}{a} \sinh \frac{2n\pi z}{a} \quad (10)$$

Parallel to the X-axis in figure 2, the field changes periodically. This suggests that the field can be expressed as a Fourier series. (Indeed, any valid solution to Laplace's equation can be expressed as a Fourier series.) Equation (10) has the form of the nth term of such a series, which might look like the following:

$$\phi = \sum_{n=1}^{\infty} D_n \cos \frac{2n\pi x}{a} \sinh \frac{2n\pi z}{a} \quad (11)$$

At large distances from the grid, the potential must approach that of a uniform charge distribution. That is, in the region between the grid and the plate, as  $z/a$  approaches zero the potential must approach a linear function of  $z$ . This function  $\phi_0(z)$  is the potential corresponding to the constant electric field that would exist at large distances from the grid. Equation (11) is modified to include the  $\phi_0(z)$  term:

$$\phi = \phi_0(z) + \sum_{n=1}^{\infty} D_n \cos \frac{2n\pi x}{a} \sinh \frac{2n\pi z}{a} \quad (12)$$

The function  $\phi_0(z)$  is linear in  $z$ , does not depend on  $x$ , and is zero when  $z = 0$ . When  $z/a$  approaches zero, the oscillating terms in the sum approach zero and the potential approaches  $\phi_0$  as required.

Equation (12) still satisfies Laplace's equation. Now  $D_n$  and  $\phi_0(z)$  must be determined so that equation (12) will meet the boundary conditions. Before  $D_n$  and  $\phi_0$  can be found, the boundary conditions must be established.

The potential is zero at  $z = 0$  by the way the problem is set up. Since  $\phi_0(z=0) = 0$  by definition, equation (12) already satisfies the lower boundary condition. The potential on the upper boundary is  $V$  wherever there is a wire and something less than  $V$  in the space between the wires. Figure 3 is a schematic representation of the potential in the  $z = b$  plane.

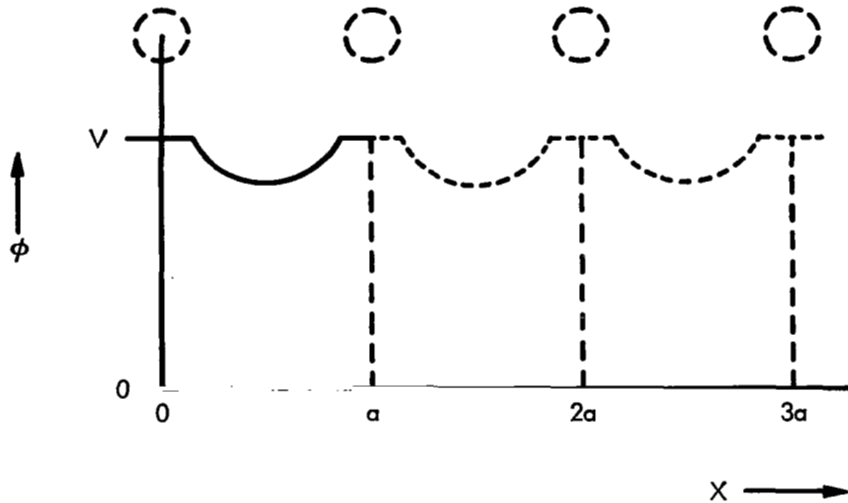


Figure 3.- Potential at upper boundary.

Since  $\phi(x,b)$  is a periodic function, it can be evaluated over the range  $0 \leq x \leq a$  and expanded in a Fourier series. The potential over the range  $0 \leq x \leq a$  is the potential corresponding to a parallel array of wires of radius  $r$  separated center-to-center by a distance  $a$  with charge residing on one side of the wires (because of the influence of the grounded plate). The potential is considered only on the line connecting the centers of the wires (the  $z = b$  plane).

The method of images will be used to solve the field of a grounded plate near an array of parallel charged wires. The potential of an array of parallel charged wires in the presence of a grounded plate is the same as that of an array of parallel line charges, each one corresponding to the axial center of charge of one of the wires. If the grounded plate is replaced by a parallel array of image line charges, as in figure 4, the field is unchanged. For each wire, the location of the axial center of charge will depend on the wire radius and on the wire-plate separation. If the distance between each wire and the grounded plate is very large, the center of charge can be said to correspond to the axis of the wire. If the wire-plate separation is vanishingly small, the axial center of charge for each wire will approach the bottom edge of the wire.

In figure 4,  $\delta$  represents the distance that the axis of charge of each wire is displaced from the geometric axis of the wire due to the influence of the grounded plate. Consider the potential at point  $P(x,b)$ , which lies in the plane of the grid. The potential at  $P(x,b)$  is composed of contributions from all the line charges and image line charges. If  $d_n$  represents the distance from point  $P$  to the  $n$ th line charge and  $d_n'$  represents the distance from point  $P$  to the  $n$ th image line charge, they can be expressed by

$$d_n = \sqrt{(x - na)^2 + \delta^2} \qquad d_n' = \sqrt{(x - na)^2 + (2b - \delta)^2}$$

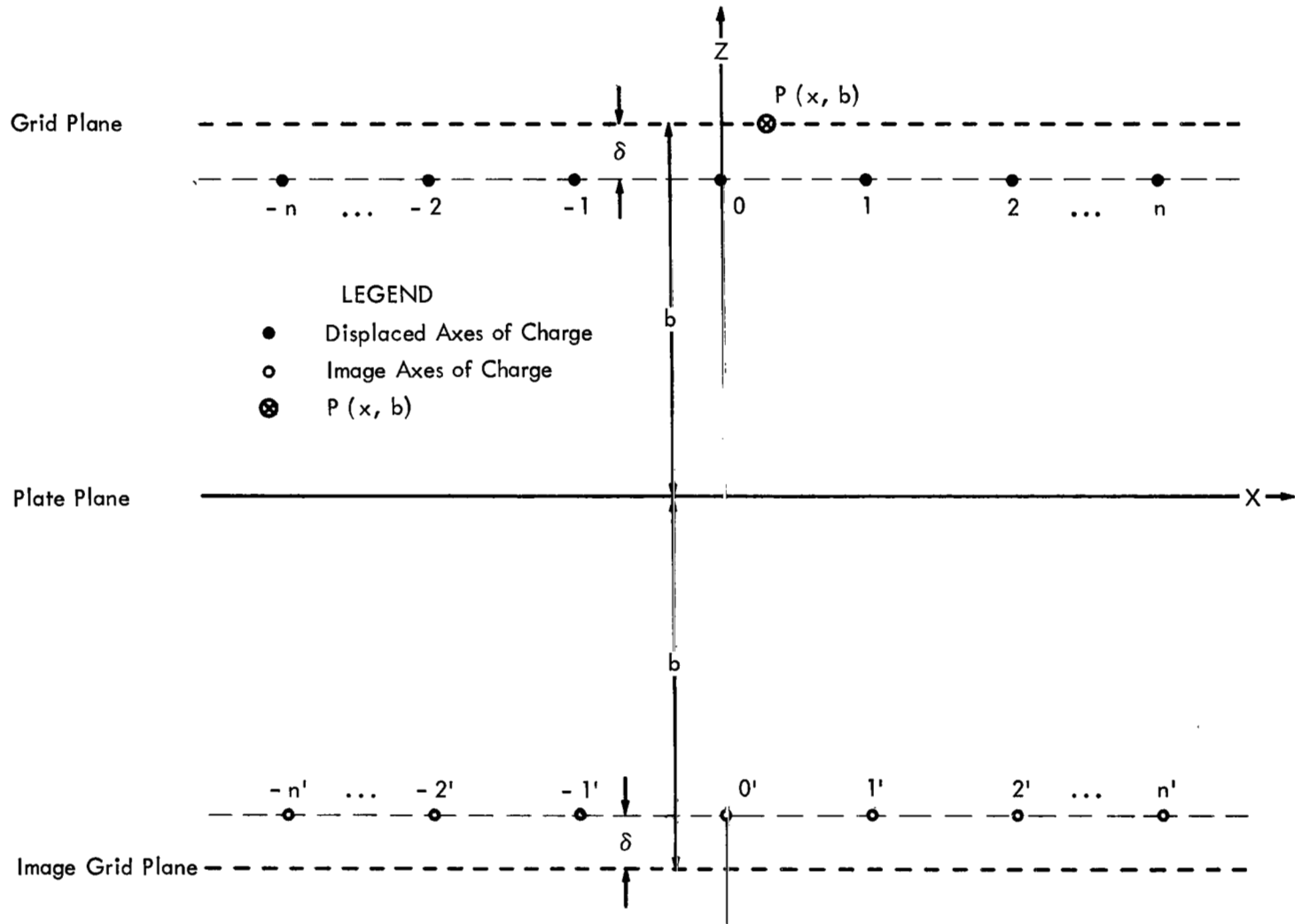


Figure 4.- Image line charge distribution of a charged grid and grounded plate.

Both of these expressions hold for positive and negative  $n$ . The potential of a line charge can be shown to be

$$\phi = -\frac{\lambda}{2\pi\epsilon} \ln d + \text{Const.}$$

where  $\lambda$  is the linear charge density,  $d$  is the radial distance from the line charge, and the arbitrary constant defines the zero of potential. Therefore the potential at point  $P$  due to the  $n$ th line charge is

$$\phi_n = -\frac{\lambda}{2\pi\epsilon} \ln d_n + \text{Const.}$$

and the potential at point  $P$  due to the  $n$ th image line charge is

$$\phi_n' = \frac{\lambda}{2\pi\epsilon} \ln d_n' + \text{Const.}$$

The potential at point  $P$  is then found by superposing the  $\phi_n$  and  $\phi_n'$  values:

$$\begin{aligned} \phi(x,b) &= \frac{\lambda}{4\pi\epsilon} \sum_{n=-\infty}^{+\infty} \left\{ \ln \left[ (x - na)^2 + (2b - \delta)^2 \right]^{1/2} - \ln \left[ (x - na)^2 + \delta^2 \right]^{1/2} \right\} + \text{Const.} \\ &= \frac{\lambda}{8\pi\epsilon} \sum_{n=-\infty}^{+\infty} \ln \frac{(x - na)^2 + (2b - \delta)^2}{(x - na)^2 + \delta^2} + \text{Const.} \end{aligned} \quad (13)$$

or, finally,

$$\phi(x,b) = \frac{\lambda}{8\pi\epsilon} \ln \left\{ \prod_{n=-\infty}^{+\infty} \left[ 1 + \frac{4b(b - \delta)}{(x - na)^2 + \delta^2} \right] \right\} + \text{Const.} \quad (14)$$

The maximum value of  $\delta$  is  $r$ , the wire radius, corresponding to the case when the plate is almost touching the grid of wires. Of course, the minimum value of  $\delta$  is zero, when the plate is far away from the grid. If  $a^2 \gg r^2$  (which is true for a large-mesh grid of fine wires),  $\delta$  can be neglected in equation (14) for all cases except the  $n = 0$  case. Since  $x$  can be as small as  $r$  ( $\phi$  is defined by eq. (14) in the region between adjacent wires) and since  $\delta$  can be as large as  $r$  (corresponding to a vanishingly small grid-plate separation), it is not immediately obvious that  $\delta$  can be neglected in equation (14) if  $n = 0$ . In appendix A it is shown that even when the plate is close to the axis of the wires, neglecting  $\delta$  in equation (14) introduces a negligible error in the

$n = 0$  term. The error introduced in the other terms of equation (14) will be even less. Therefore,  $\delta$  is dropped from equation (14). With  $\delta$  assumed to be zero for all practical purposes, equation (14) can be restated as follows:

$$\phi(x,b) = \frac{\lambda}{8\pi\epsilon} \ln \left\{ \prod_{n=-\infty}^{+\infty} \left[ 1 + \left( \frac{2b}{x - na} \right)^2 \right] \right\} + \text{Const.} \quad (15)$$

This infinite product can be expressed in closed form (ref. 11) as follows:

$$\prod_{n=-\infty}^{+\infty} \left[ 1 + \left( \frac{2b}{x - na} \right)^2 \right] = \frac{\cosh 2\alpha b - \cos \alpha x}{1 - \cos \alpha x} \quad (16)$$

where  $\alpha = \frac{2\pi}{a}$ .

Equation (14) thus becomes:

$$\phi(x,b) = \frac{\lambda}{8\pi\epsilon} \left( \ln \frac{\cosh 2\alpha b - \cos \alpha x}{1 - \cos \alpha x} \right) + \text{Const.} \quad (17)$$

To evaluate the constant, consider the fact that when  $x = r$ ,  $\phi(x,b)$  must be  $V$ , the potential of the wire:

$$\phi(r,b) = V = \frac{\lambda}{8\pi\epsilon} \left( \ln \frac{\cosh 2\alpha b - \cos \alpha r}{1 - \cos \alpha r} \right) + \text{Const.}$$

Thus

$$\text{Const.} = V - \frac{\lambda}{8\pi\epsilon} \ln \frac{\cosh 2\alpha b - \cos \alpha r}{1 - \cos \alpha r}$$

Then

$$\phi(x,b) = \frac{\lambda}{8\pi\epsilon} \left( \ln \frac{\cosh 2\alpha b - \cos \alpha x}{1 - \cos \alpha x} \right) + V - \frac{\lambda}{8\pi\epsilon} \ln \frac{\cosh 2\alpha b - \cos \alpha r}{1 - \cos \alpha r} \quad (18)$$

or

$$\phi(x,b) = V + \frac{\lambda}{8\pi\epsilon} \ln \frac{(\cosh 2\alpha b - \cos \alpha x)(1 - \cos \alpha r)}{(\cosh 2\alpha b - \cos \alpha r)(1 - \cos \alpha x)} \quad (19)$$

Of course, equation (19) holds only between the wires since the potential inside a conductor must be the same as the potential on the surface. The potential inside the wires ( $0 < x < r$  and  $(a-r) < x < a$ ) is  $V$ . Therefore, for  $0 < x < a$ ,  $\phi(x,b)$  is as follows:

$$\phi(x,b) = \begin{cases} V & (0 \leq x \leq r) \\ V + \frac{\lambda}{8\pi\epsilon} \ln \frac{(\cosh 2\alpha b - \cos \alpha x)(1 - \cos \alpha r)}{(\cosh 2\alpha b - \cos \alpha r)(1 - \cos \alpha x)} & [r \leq x \leq (a-r)] \\ V & [(a-r) \leq x \leq a] \end{cases} \quad (20)$$

In equation (12) the potential distribution was cast in the form of a Fourier cosine series with two as yet unidentified constants. In order to evaluate these constants, equation (20) is expanded in a Fourier cosine series and compared term by term with equation (12). The expansion is carried out in appendix B with the following result:

$$\begin{aligned} \phi(x,b) = & V \left\{ 1 - \frac{4Tr}{a} + T \left[ \frac{\cos \alpha r}{\cosh 2\alpha b} + 2 \ln \left( 2 \sin \frac{\alpha r}{2} \right) \right] \right\} \\ & + \left\{ \frac{2VT [\pi - 2 \text{Si}(\alpha r)]}{\pi} - \frac{VT}{\cosh 2\alpha b} \right\} \cos \alpha x \\ & + \sum_{n=2}^{\infty} \frac{2VT}{\pi} \frac{\pi - 2 \text{Si}(n\alpha r)}{n} \cos n\alpha x \end{aligned} \quad (21)$$

where

$$T = \frac{\lambda}{8\pi\epsilon V} \quad \alpha = \frac{2\pi}{a} \quad \text{Si}(n\alpha r) = \int_{x=0}^{x=n\alpha r} \frac{\sin x}{x} dx$$

Equation (21) represents the grid-plate potential distribution in the plane of the grid. It is the upper boundary condition. That is, when equation (12) is evaluated at  $z = b$  (the plane of the grid) the constants  $\phi_0$  and  $D_n$  must be such that equation (12) and equation (21) are identical. Note that the upper boundary has been expressed as the sum of a  $\phi_0$  term, a  $\phi_1$  term, and an infinite series of terms  $\phi_n$ , where  $n \geq 2$ . This is simply because equation (20) was taken as the sum of three functions, and the Fourier cosine expansion of one of them contained only two terms (see appendix C). It is therefore necessary to express equation (12), the general solution, in a form similar to equation (21) in order to evaluate the unknown coefficients. Clearly, equation (12) can be expressed as follows:

$$\phi(x,z) = \phi_0(z) + D_1 \cos \frac{2\pi x}{a} \sinh \frac{2\pi z}{a} + \sum_{n=2}^{\infty} D_n \cos \frac{2n\pi x}{a} \sinh \frac{2n\pi z}{a} \quad (22)$$

Consider this expression at  $z = b$ :

$$\phi(x,b) = \phi_0(b) + D_1 \cos \frac{2\pi x}{a} \sinh \frac{2\pi b}{a} + \sum_{n=2}^{\infty} D_n \cos \frac{2n\pi x}{a} \sinh \frac{2n\pi b}{a} \quad (23)$$

This is just the general solution of the potential problem evaluated at the upper boundary. If equation (23) is compared term by term with equation (21), the upper boundary condition, the following equalities are identified:

$$\phi_0(b) = V \left\{ 1 - \frac{4Tr}{a} + T \left[ \frac{\cos \alpha r}{\cosh 2\alpha b} + 2 \ln \left( 2 \sin \frac{\alpha r}{2} \right) \right] \right\}$$

$$D_1 \cos \frac{2\pi x}{a} \sinh \frac{2\pi b}{a} = \left\{ \frac{2VT [\pi - 2 \text{Si}(\alpha r)]}{\pi} - \frac{VT}{\cosh 2\alpha b} \right\} \cos \alpha x$$

$$D_n \cos \frac{2n\pi x}{a} \sinh \frac{2n\pi b}{a} = \frac{2VT}{\pi} \frac{\pi - 2 \text{Si}(n\alpha r)}{n} \cos n\alpha x$$

Since  $\alpha = \frac{2\pi}{a}$ , these equations can be written as

$$\phi_0(z) = V \left\{ 1 - \frac{4Tr}{a} + T \left[ \frac{\cos \alpha r}{\cosh 2\alpha b} + 2 \ln \left( 2 \sin \frac{\alpha r}{2} \right) \right] \right\} \frac{z}{b} \quad (24)$$

$$D_1 = \frac{VT}{\sinh \alpha b} \left\{ \frac{2 [\pi - 2 \text{Si}(\alpha r)]}{\pi} - \frac{1}{\cosh 2\alpha b} \right\} \quad (25)$$

$$D_n = \frac{2VT}{\sinh n\alpha b} \frac{\pi - 2 \text{Si}(n\alpha r)}{n\pi} \quad (n \geq 2) \quad (26)$$

Equations (24) to (26) are inserted into equation (22) to yield the general solution of the potential problem in two dimensions:

$$\begin{aligned}
\phi(x,z) = V & \left\{ 1 - \frac{4Tr}{a} + T \left[ \frac{\cos \alpha r}{\cosh 2\alpha b} + 2 \ln \left( 2 \sin \frac{\alpha r}{2} \right) \right] \right\} \frac{z}{b} \\
& + \frac{VT}{\sinh \alpha b} \left\{ \frac{2[\pi - 2 \text{Si}(\alpha r)]}{\pi} - \frac{1}{\cosh 2\alpha b} \right\} \sinh \alpha z \cos \alpha x \\
& + \frac{2VT}{\pi} \sum_{n=2}^{\infty} \frac{\pi - 2 \text{Si}(n\alpha r)}{n} \frac{\sinh n\alpha z}{\sinh n\alpha b} \cos n\alpha x
\end{aligned} \tag{27}$$

This is the solution to the problem in two dimensions, but the actual grid consists of a plate and two perpendicular arrays of parallel wires. The solution to the three-dimensional problem is thus a superposition of a pair of two-dimensional solutions. That is,  $\phi(x,y,z)$  is in reality  $\phi(x,z)$  (eq. (27)) superimposed with the following equation for  $\phi(y,z)$  (eq. (27) with  $x$  replaced by  $y$ ):

$$\begin{aligned}
\phi(y,z) = V & \left\{ 1 - \frac{4Tr}{a} + T \left[ \frac{\cos \alpha r}{\cosh 2\alpha b} + 2 \ln \left( 2 \sin \frac{\alpha r}{2} \right) \right] \right\} \frac{z}{b} \\
& + \frac{VT}{\sinh \alpha b} \left\{ \frac{2[\pi - 2 \text{Si}(\alpha r)]}{\pi} - \frac{1}{\cosh 2\alpha b} \right\} \sinh \alpha z \cos \alpha y \\
& + 2VT \sum_{n=2}^{\infty} \frac{\pi - 2 \text{Si}(n\alpha r)}{n\pi} \frac{\sinh n\alpha z}{\sinh n\alpha b} \cos n\alpha y
\end{aligned} \tag{28}$$

The  $\phi_0$  term is unaffected by the superposition. It is just the potential which exists at large distances from the grid where the oscillating terms in the series do not add appreciably to the potential; that is, it corresponds to the uniform charge distribution which the grid appears to have at large distances from it. For a given  $z$ ,  $\phi_0$  is a function only of the charge density and since superimposing two similar (perpendicular) wire arrays does not change the overall charge density of the grid, the  $\phi_0$  term remains unaffected. When  $\phi(x,z)$  and  $\phi(y,z)$  are superimposed, the result is as follows:

$$\begin{aligned}
\phi(x,y,z) = V & \left\{ 1 - \frac{4Tr}{a} + T \left[ \frac{\cos \alpha r}{\cosh 2\alpha b} + 2 \ln \left( 2 \sin \frac{\alpha r}{2} \right) \right] \right\} \frac{z}{b} \\
& + \frac{VT}{\sinh \alpha b} \left\{ \frac{2[\pi - 2 \text{Si}(\alpha r)]}{\pi} - \frac{1}{\cosh 2\alpha b} \right\} \sinh \alpha z (\cos \alpha x + \cos \alpha y) \\
& + \frac{2VT}{\pi} \sum_{n=2}^{\infty} \frac{\pi - 2 \text{Si}(n\alpha r)}{n} \frac{\sinh n\alpha z}{\sinh n\alpha b} (\cos n\alpha x + \cos n\alpha y)
\end{aligned} \tag{29}$$

Equation (29) describes the potential distribution that exists between a flat grounded plate and a square-mesh grid of wires charged to some potential  $V$  with respect to the plate. All the parameters are easily measured except  $T$ , which is defined by

$$T = \frac{\lambda}{8\pi\epsilon V}$$

It would be most convenient to be able to express  $\lambda$  in terms of some easily measured parameters. This can be done as follows. The capacitance of a system consisting of a long charged wire parallel to an infinite grounded plate is

$$C = \frac{q}{V}$$

where  $q$  is the excess charge on the wire and  $V$  the potential difference between the wire and the plate. From this it follows that

$$C_l = \frac{\lambda}{V}$$

where  $C_l$  is the capacitance per unit length of the system. Thus the linear charge density of a charged wire in the presence of a grounded plate is

$$\lambda = VC_l$$

The capacitance per unit length of a wire-plate system is (ref. 12)

$$C_l = \frac{2\pi\epsilon}{\ln \left[ \frac{1}{r} \left( \sqrt{b^2 - r^2} + b \right) \right]} \quad (30)$$

Thus

$$\lambda = \frac{2\pi\epsilon V}{\ln \left[ \frac{1}{r} \left( \sqrt{b^2 - r^2} + b \right) \right]} \quad (31)$$

and

$$T = \frac{1}{4 \ln \left[ \frac{1}{r} \left( \sqrt{b^2 - r^2} + b \right) \right]} \quad (32)$$

Equation (32) can be inserted into equation (29) to find the potential distribution of a charged grid-plate capacitor in terms of easily measured parameters, namely the grid-plate spacing  $b$ , the parallel-wire separation  $a$ , the wire radius  $r$ , and the grid-plate potential difference  $V$ .

### Computation of Capacitance From Potential

The fact that the capacitance between arbitrarily shaped conductors can be derived from the potential distribution that exists when the conductors are charged was discussed in the section entitled "Approach." The relation between capacitance and potential was expressed in equation (2):

$$C = \frac{\epsilon}{V^2} \int_{\tau} (\nabla\phi)^2 d\tau$$

This volume integral is taken throughout the region bounded by the conductors. An expression for  $\phi$  is derived in the previous section (eq. (29)), and in appendix C this expression is inserted into equation (2) to yield

$$C = \frac{LW\epsilon}{b} \left( A_0^2 + \sum_{n=1}^{\infty} A_n^2 \frac{n\alpha b \sinh 2n\alpha b}{2} \right) \quad (33)$$

where

$$A_0 = 1 - \frac{4rT}{a} + T \left[ \frac{\cos \alpha r}{\cosh 2\alpha b} + 2 \ln \left( 2 \sin \frac{\alpha r}{2} \right) \right]$$

$$A_1 = \frac{T}{\sinh \alpha b} \left\{ \frac{2 [\pi - 2 \text{Si}(\alpha r)]}{\pi} - \frac{1}{\cosh 2\alpha b} \right\}$$

$$A_n = \frac{2T}{\sinh n\alpha b} \frac{\pi - 2 \text{Si}(n\alpha r)}{n\pi} \quad (n \geq 2)$$

$$\alpha = \frac{2\pi}{a}$$

$$T = \frac{1}{4 \ln \left[ \frac{1}{r} \left( \sqrt{b^2 - r^2} + b \right) \right]}$$

Note that in equation (33) the term outside the parentheses is the formula for the capacitance of a parallel solid-plate capacitor with plate dimensions  $L$  and  $W$  and separation distance  $b$ . The term in parentheses is a measure of how this capacitance is changed when one of the plates is replaced by a square-mesh grid of wires with radius  $r$  separated axis-to-axis a distance  $a$ .

It should be remembered that the expression used for the potential distribution to determine the capacitance was only an approximate one. Although the capacitance formula is derived by a variational method that requires only an approximate expression for  $\phi$  to yield a very close approximation to the true capacitance, nevertheless equation (33) represents only an approximation to the true grid-plate capacitance. Just how good this approximation is can be determined by actually measuring the capacitance of a number of grid-plate configurations and comparing the results with predictions based on equation (33). Values reported in the next section reflect equation (33) carried out (by computing calculator) to 15 terms. Actually, the series in equation (33) converges quite rapidly, and very good results can be had by retaining fewer terms in the series.

#### EXPERIMENTAL CONFIRMATION OF THEORY

Capacitance measurements were made on a number of grid-plate configurations. The grid-plate capacitors were composed of a single flat polished plate of aluminum and a number of interchangeable grids. Each grid in turn was positioned above the aluminum plate by means of a number of columns of small cardboard spacers, which varied in height from 5.1 mm to 12.7 mm in 1.3-mm increments. Several data points were taken for each grid, every point corresponding to a different grid-plate separation. Thus, for each grid, an experimental curve of capacitance as a function of grid-plate separation was generated. A theoretical curve was obtained by programming the capacitance formula on a computer with instructions to increment  $b$ , the grid-plate separation parameter. Each computer-generated data point was also plotted. Comparisons between the empirical and theoretical curves indicate that the grid-plate capacitance formula is exact within experimental error.

Figure 5 illustrates a typical experimental configuration. The flat plate is mounted on a hollow block of polystyrene to displace it from the table and reduce the effect of stray capacitance. The spacers are positioned on the plate and the grid is placed on top of the spacers. The spacers were positioned so as to prevent the grid from sagging. End effects were suppressed by using relatively small grid-plate separation distances and relatively large grids and plates (ratios of plate area to separation on the order of 500 to 1). The capacitance measurements were made with a precision industrial capacitance bridge. The recorded data, corrected for effects of the cardboard spacers, fringing fields, and meter-lead capacitance, are reported in tables I and II for two grid-plate capacitors. In each case, predicted and measured values are given for a number of grid-plate separations.

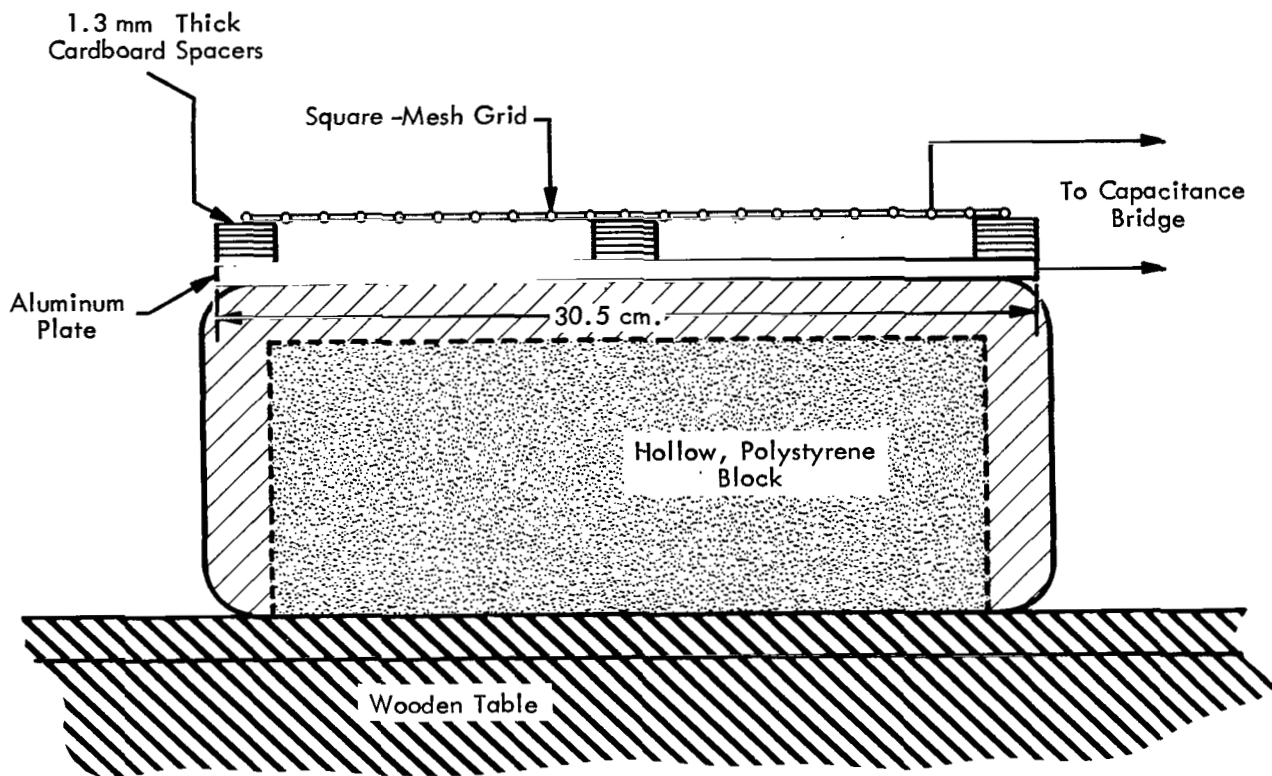


Figure 5.- Configuration for capacitance measurements.

TABLE I.- 6.4-mm MESH

Wire radius,  $0.318 \text{ mm} \pm 0.013$   
 Mesh dimension,  $6.350 \text{ mm} \pm 0.025$   
 Edge of grid and plate,  $30.5 \text{ cm} \pm 0.1$   
 Spacer thickness (each),  $1.270 \text{ mm} \pm 0.010$

Number of spacers	Grid-plate capacitance, picofarads	
	Experimental	Theory
4	$139.8 \pm 1.5$	$142.8 \pm 3.5$
5	$116.3 \pm 1.9$	$116.4 \pm 0.3$
6	$99.7 \pm 0.8$	$100.3 \pm 0.7$
7	$88.2 \pm 1.0$	$88.7 \pm 1.0$
8	$79.0 \pm 0.6$	$79.1 \pm 0.3$
10	$66.0 \pm 0.6$	$65.3 \pm 0.5$

TABLE II.- 25.4-mm MESH

Wire radius,  $0.635 \text{ mm} \pm 0.051$   
 Mesh dimension,  $25.400 \text{ mm} \pm 0.102$   
 Edge of grid and plate,  $30.5 \text{ cm} \pm 0.1$   
 Spacer thickness (each),  $1.270 \text{ mm} \pm 0.010$

Number of spacers	Grid-plate capacitance, picofarads	
	Experimental	Theory
4	$108.3 \pm 6.5$	$102.8 \pm 1.3$
5	$95.3 \pm 2.0$	$90.2 \pm 1.0$
6	$83.9 \pm 2.1$	$81.1 \pm 0.9$
7	$74.7 \pm 1.5$	$74.0 \pm 0.7$
8	$68.0 \pm 1.1$	$68.4 \pm 0.8$
9	$61.4 \pm 0.8$	$63.8 \pm 0.7$
10	$58.0 \pm 0.8$	$60.0 \pm 0.7$

Figures 6 and 7 are computer-generated curves of the capacitance formula, equation (33), as applied to the grid-plate capacitors described in tables I and II. Superimposed on the theoretical curves are measured data points, with error bars.

## DISCUSSION OF RESULTS

All the uncertainties in the experimental values reported, both in geometric measurements and measurements of capacitance, are the standard deviations based on 10 measurements per point. Uncertainties in the theory reflect the standard deviations in measured grid-plate geometry parameters.

In the theoretical analysis, the thin-wire approximation was made a number of times. Hence, the analysis can be accurately applied only to geometries in which the radius of the grid wires is small compared with other dimensions such as the grid-plate spacing and the distance between adjacent parallel wires.

The charge distribution on each wire is slightly affected by the presence of charge on neighboring wires, if the grid is assumed to be finite. However, the effect is quite small everywhere except near the very edges of the condenser, and even there the effect is small for thin wires, since the center of charge of each wire is constrained to lie somewhere inside the wire.

The axial center of charge of each wire in the grid was assumed to coincide with the geometric axis of each wire. Because of the influence of the grounded plate, this is not really the case; the charge is shifted slightly toward the plate. However, it is shown in appendix A that even when the plate is very close to the grid, the shift in the axial center of charge is quite small and can in fact be neglected for a wide range of grid-plate separations.

In making the capacitance measurements, the grid of each grid-plate condenser was suspended over the plate by means of cardboard spacers. Care was taken in the placement of the spacers to minimize the effects of sag in the grid; however, the data may be biased slightly high where the grid-plate spacing is relatively small and grid sag would have a larger percentage effect. Care was also taken to minimize the effects of stray capacitance by isolating the grid-plate condensers as much as possible; however, some small stray capacitance effects are inevitable. They would also tend to bias the data slightly high. Finally, the grids used in the measurements were made out of metal which had been dipped in a galvanizing solution. Consequently, there were some irregularities in the grid, especially at the wire intersections where the galvanizing solution tended to concentrate. In measuring the wire radii, several measurements were made with a micrometer at different places on the wire and the numbers listed for wire radii are average values.

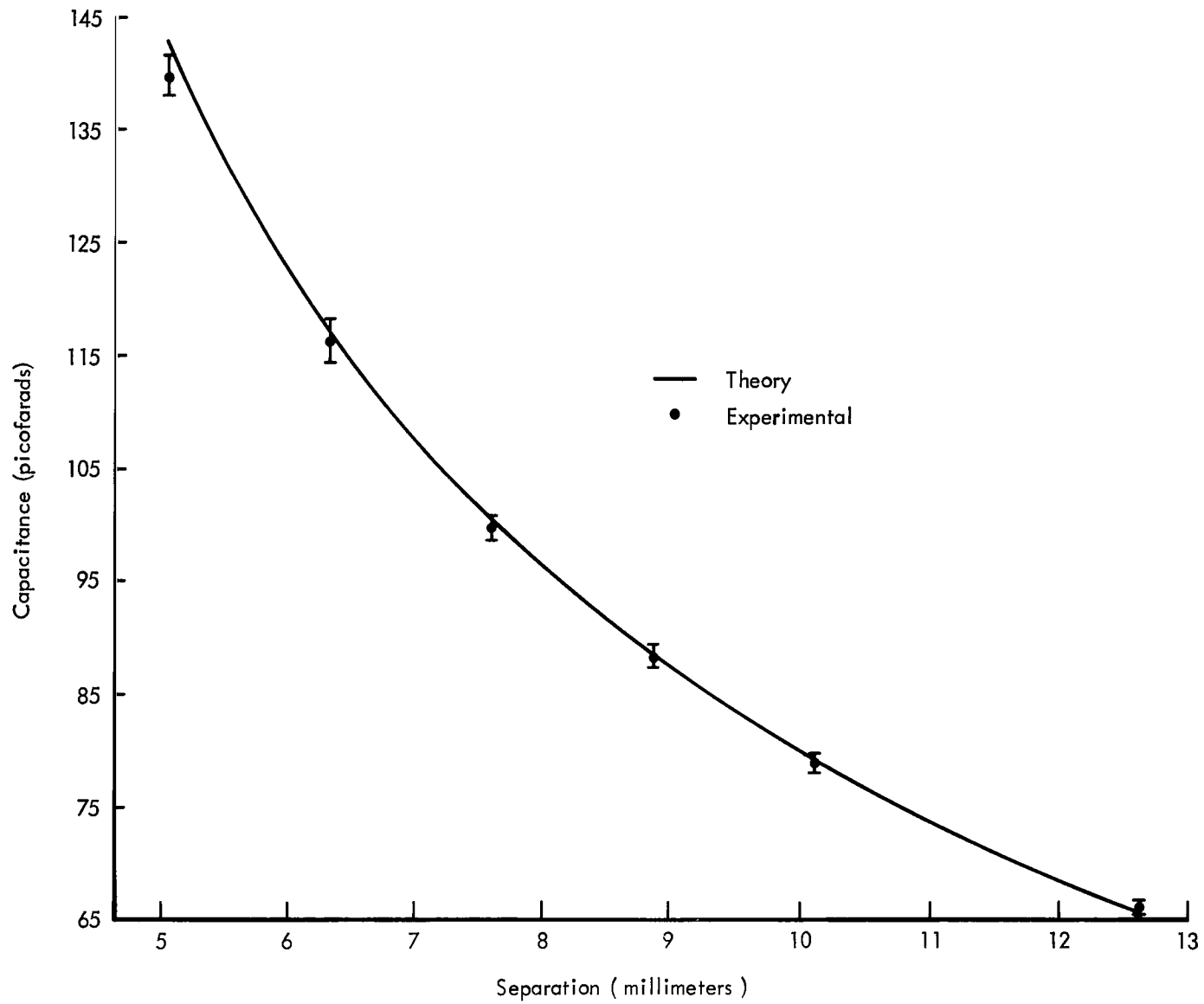


Figure 6.- Grid-plate capacitance as a function of grid-plate separation for 6.4-mm mesh.

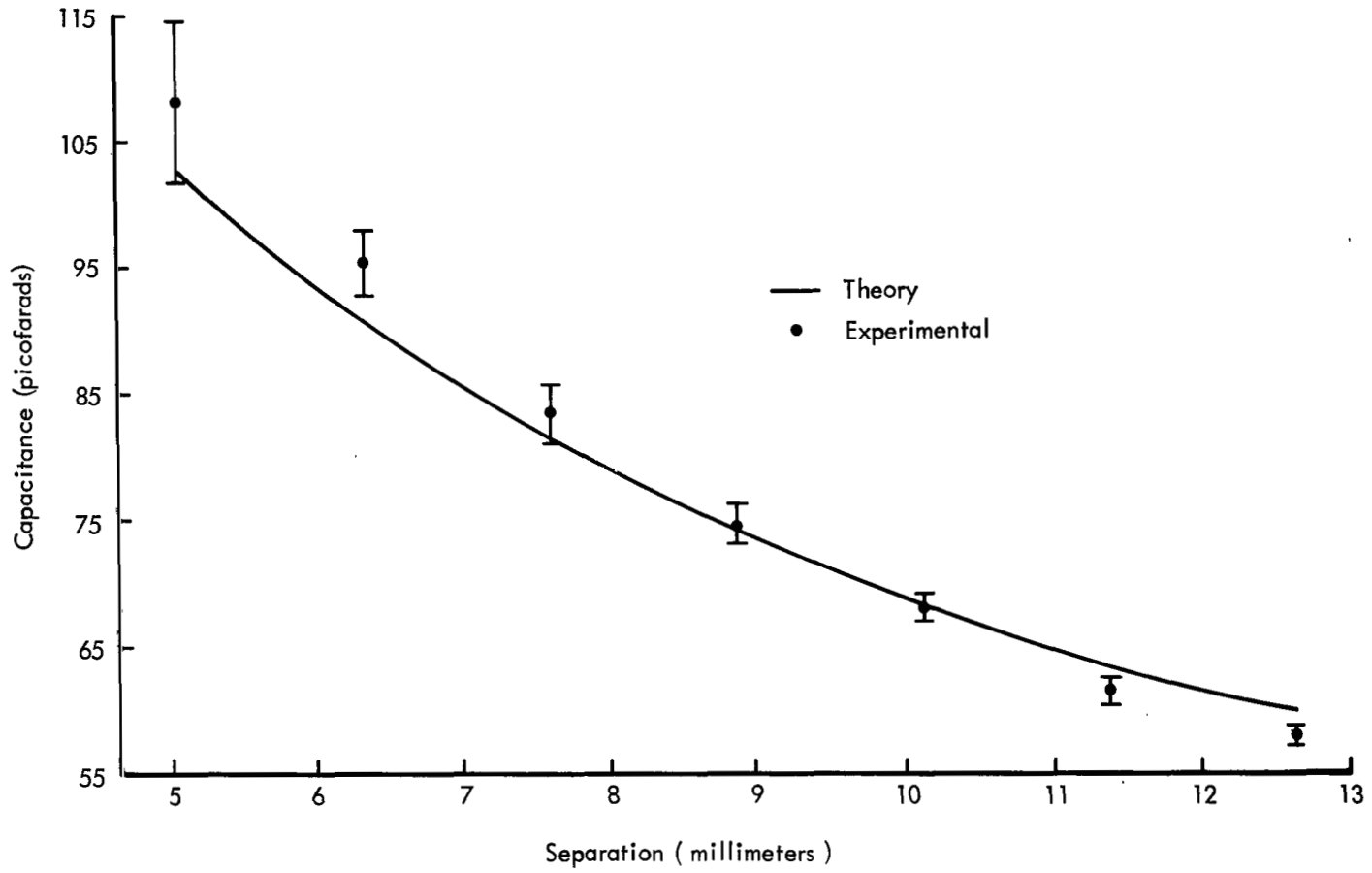


Figure 7.- Grid-plate capacitance as a function of grid-plate separation for 25.4-mm mesh.

These errors are all small, and care has been taken to minimize them. In any case, some of the errors tend to cancel so that the cumulative effect of all the error sources is very small.

The theory predicts a slightly modified inverse-first-power dependence of grid-plate capacitance on grid-plate separation, which is verified by the experimental data. This result is not surprising, since the parallel grid-plate capacitor is in effect a parallel solid-plate capacitor with one plate possessing a diminished surface area. Even though the shape of the curve of capacitance as a function of separation is not surprising, the magnitudes of the capacitance values predicted (and measured) are quite unexpected. This is because the relative surface area of a fine-wire open-mesh grid is essentially negligible compared with the surface area of a solid plate that has the same length and width. Since the capacitance of a parallel-plate capacitor is directly proportional to the surface area of the plates, replacing one of the plates with an open-mesh grid of wires having a relatively minute surface area would be expected to cause a drastic reduction in the capacitance. Such was not found to be the case. Table III compares measured capacitance values from tables I and II with a parallel solid-plate condenser of the same length and width. Figure 8 is a graph of these data.

TABLE III.- CONDENSER COMPARISONS

Number of 1.3-mm spacers	Capacitance, picofarads		
	25.4-mm mesh	6.4-mm mesh	Parallel plate
4	108.3	139.8	188.6
5	95.3	116.3	143.8
6	83.9	99.7	120.4
7	74.7	88.2	103.2
8	68.0	79.0	92.0
9	61.4	71.2	82.0
10	58.0	66.0	74.5

These data illustrate that the capacitance between a plate and an open-mesh grid is surprisingly similar in magnitude to the capacitance of a parallel solid-plate condenser even when the surface area of the mesh is less by orders of magnitude than the plate area. This has led to the conclusion that the minute surface areas which characterize such open-mesh structures as the LOFT radio telescope (described in the introduction) do not impose a serious restriction on the use of capacitive, noncontacting displacement-measuring transducers in the modal analysis of the dynamic response of such structures.

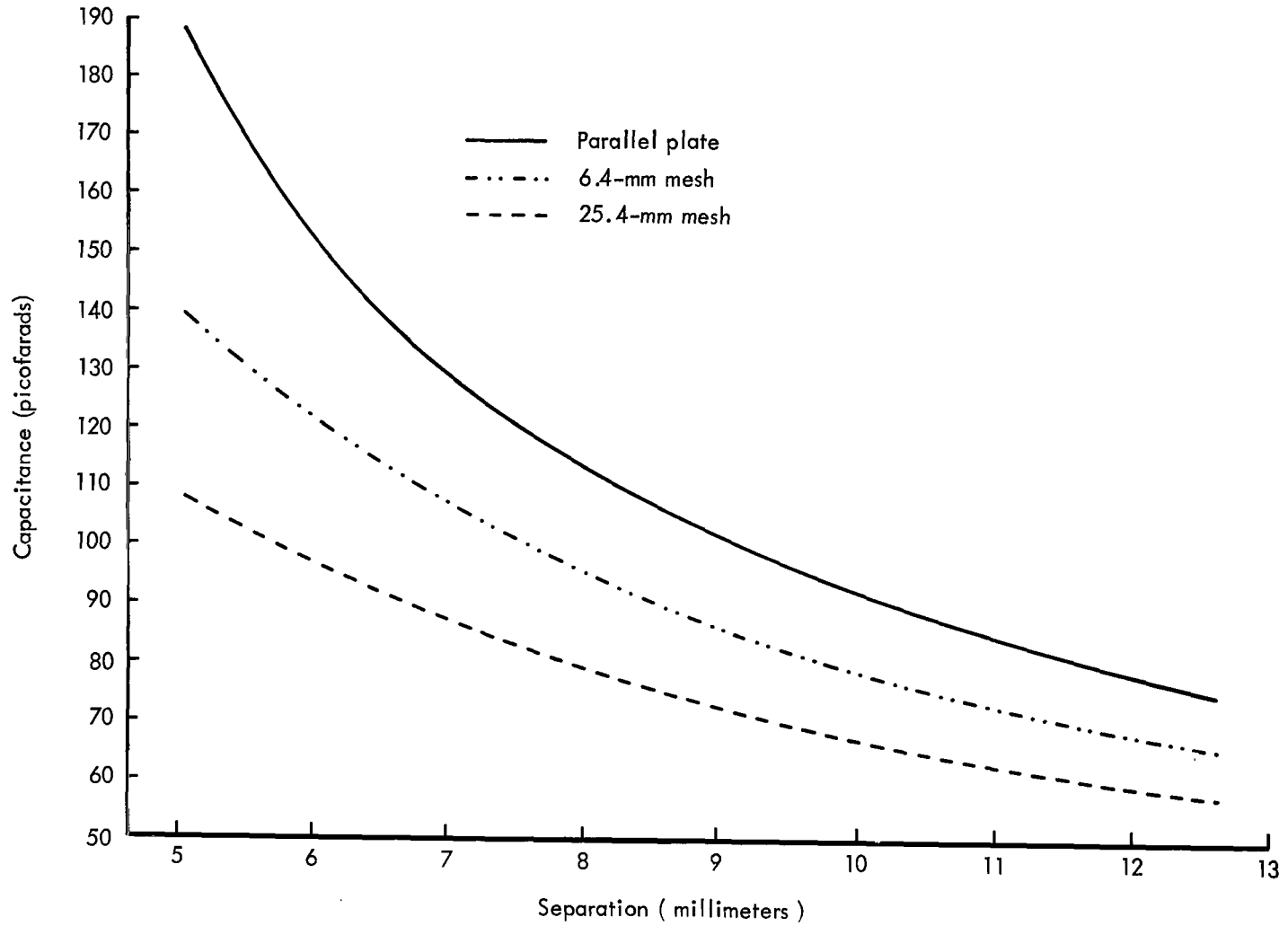


Figure 8. - Comparison of experimental capacitance values of parallel solid-plate and grid-plate capacitors.

## POTENTIAL APPLICATION

A laboratory prototype capacitive transducer system has been developed for application to the LOFT structural-stability tests mentioned in the introduction. In laboratory prototype testing, a 15-cm-diameter circular probe mounted 30 cm from the LOFT reflector net has detected displacements of the net in the range from 0.05 cm to 20 cm. Deflections in the LOFT reflector net on the order of 0.2 cm have been detected from as far away as 75 cm. Development of calibration techniques and further refinements would be required prior to application of this instrument system. Other potential applications include vibratory and modal analysis of small-surfaced hot structures and displacement measurements on fragile or lightweight surfaces in general.

## CONCLUDING REMARKS

The purpose of this paper has been to demonstrate the feasibility of employing a capacitive displacement-measuring transducer in the modal analysis of open-mesh grid structures possessing minute surface areas. The analysis has been centered about a mathematical model of a square-mesh parallel grid-plate capacitor. An expression for the capacitance of such a capacitor was derived, and values based on this expression were verified by experiment. It has been concluded that the capacitance between a flat plate and an open-mesh grid of fine wires is of sufficient magnitude to justify the development of a capacitive transducer for application to displacement-measurement problems involving open-mesh structures. A program has been initiated to develop such a transducer, and a laboratory prototype system has been built.

Langley Research Center,  
National Aeronautics and Space Administration,  
Hampton, Va., June 23, 1971.

## APPENDIX A

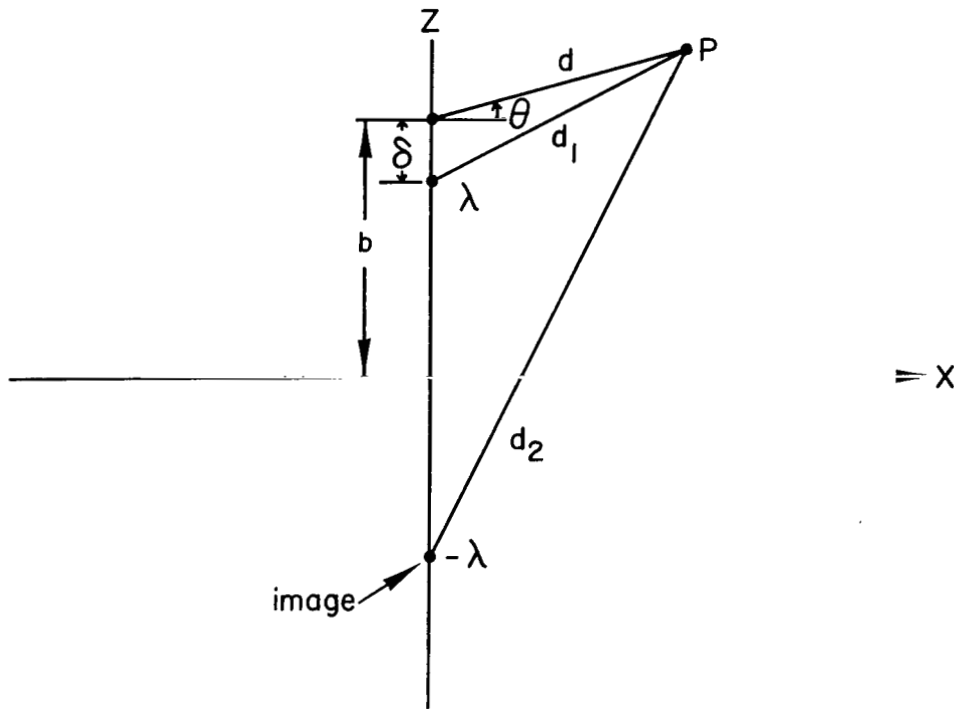
### DETERMINATION OF THE ORDER OF MAGNITUDE OF $\delta$

By Norman C. Wenger  
Lewis Research Center

The axis of charge of a long, uniformly charged wire coincides with the axis of the wire. If an infinite grounded plate is brought near a charged wire, the axis of charge will be shifted somewhat by a radial distance  $\delta$ , where  $\delta$  is greater than zero and less than the radius of the wire.

The center of the wire is assumed to be located a distance  $z = b$  above a grounded plane and the axis of charge is shifted a distance  $\delta$  below this. Then  $\delta$  is calculated by replacing the grounded plane with an image line charge (see sketch (a)):

$$\phi(P) = -\frac{\lambda}{2\pi\epsilon} \ln d_1 + \frac{\lambda}{2\pi\epsilon} \ln d_2 + \text{Const.}$$



Sketch (a)

Since  $d_1 = d_2$  at  $z = 0$ , it follows that  $\phi(z=0) = 0$  for all  $x$ , and hence the constant equals zero. Then

APPENDIX A – Continued

$$\phi(P) = \frac{\lambda}{2\pi\epsilon} \ln \frac{d_1}{d_2}$$

When  $d_2/d_1$  is a constant,  $\phi(P)$  is a constant. The (equipotential) surface that corresponds to  $\frac{d_2}{d_1} = k$  (a constant) is determined from the following derivation:

$$d_1^2 = d^2 + \delta^2 - 2d\delta \cos\left(\theta + \frac{\pi}{2}\right)$$

$$d_2^2 = d^2 + (2b - \delta)^2 - 2d(2b - \delta)\cos\left(\theta + \frac{\pi}{2}\right)$$

$$d_1^2 = d^2 + \delta^2 - 2d\delta \sin \theta$$

$$d_2^2 = d^2 + (2b - \delta)^2 - 2d(2b - \delta)\sin \theta$$

$$d_2^2 = kd_1^2$$

$$d^2 + (2b - \delta)^2 + 2d(2b - \delta)\sin \theta = k^2d^2 + k^2\delta^2 + 2d\delta k^2\sin \theta$$

$$(1 - k^2)d^2 + (2b - \delta)^2 - k^2\delta^2 + (4b - 2\delta - 2\delta k^2)d \sin \theta = 0$$

Any value of  $k$  corresponds to an equipotential surface. If  $4b - 2\delta - 2\delta k^2 = 0$  or  $k^2 = \frac{2b - \delta}{\delta}$ , this surface is a cylinder of radius

$$r = \sqrt{\frac{(2b - \delta)^2 - k^2\delta^2}{k^2 - 1}}$$

centered at  $z = b$ . After substitution of  $k^2 = \frac{2b - \delta}{\delta}$ ,

$$r^2 = \frac{(2b - \delta)^2 - (2b - \delta)\delta}{\frac{2b - \delta}{\delta} - 1} = 2b\delta - \delta^2$$

Therefore

$$\delta^2 - 2b\delta + r^2 = 0$$

## APPENDIX A – Concluded

Solving for  $\delta$  gives

$$\delta = b \pm \sqrt{b^2 - r^2}$$

The minus sign is chosen:

$$\boxed{\delta = b - \sqrt{b^2 - r^2}}$$

The smaller the ratio  $b/r$ , the larger  $\delta$  will be. The smallest value of  $b/r$  measured in this paper corresponds to  $\delta = 0.06r$ . In the body of the paper it was necessary to compare  $r^2$  and  $\delta^2$  to see whether  $\delta^2$  was negligible when compared with  $r^2$ . In the worse case,  $\frac{\delta^2}{r^2} < 0.004$ . Clearly, then,  $1 + \frac{\delta^2}{r^2} = 1$  is a good approximation. (See eq. (14) and the discussion immediately following it.)

## APPENDIX B

### FOURIER COSINE SERIES EXPANSION OF THE TWO-DIMENSIONAL UPPER BOUNDARY CONDITION

In this appendix,  $\phi(x,b)$  as derived in equation (20) will be expanded in a Fourier cosine series. Equation (20) can be written

$$\phi(x,b) = \begin{cases} V & (0 \leq x \leq r) \\ V + VT \ln \frac{(\cosh 2\alpha b - \cos \alpha x)(1 - \cos \alpha r)}{(\cosh 2\alpha b - \cos \alpha r)(1 - \cos \alpha x)} & [r \leq x \leq (a-r)] \\ V & [(a-r) \leq x \leq a] \end{cases} \quad (B1)$$

The function  $\phi(x,b)$  has the following form:

$$\phi(x,b) = \begin{cases} V & (0 \leq x \leq r) \\ V + VTF(x) & [r \leq x \leq (a-r)] \\ V & [(a-r) \leq x \leq a] \end{cases} \quad (B2)$$

where

$$F(x) = \ln \frac{(\cosh 2\alpha b - \cos \alpha x)(1 - \cos \alpha r)}{(\cosh 2\alpha b - \cos \alpha r)(1 - \cos \alpha x)} \quad (B3)$$

A straightforward evaluation of the Fourier coefficients for the function  $\phi(x,b)$  involves the solution of some integrals that cannot be evaluated in closed form. In order to avoid this difficulty,  $\phi(x,b)$  has been synthesized from three functions which are easier to treat by Fourier analysis. The first function is called  $M(x)$  and is defined as follows:

$$M(x) = V [1 + TF(x)] \quad (0 \leq x \leq a) \quad (B4)$$

where  $F(x)$  is defined by equation (B3). The second function is  $G(x)$ :

$$G(x) = \begin{cases} M(x) & (0 \leq x \leq r) \\ 0 & [r \leq x \leq (a-r)] \\ M(x) & [(a-r) \leq x \leq a] \end{cases} \quad (B5)$$

APPENDIX B – Continued

The third function is  $H(x)$ , a simple step function:

$$H(x) = \begin{cases} V & (0 \leq x \leq r) \\ 0 & [r \leq x \leq (a-r)] \\ V & [(a-r) \leq x \leq a] \end{cases} \quad (B6)$$

Figure B1 illustrates how  $M(x)$ ,  $G(x)$ , and  $H(x)$  combine to form  $\phi(x,b)$ :

$$\phi(x,b) = M(x) - G(x) + H(x) \quad (B7)$$

The Fourier coefficients of  $M(x)$ ,  $G(x)$ , and  $H(x)$  will be derived and combined to form a Fourier series representation of  $\phi(x,b)$ .

Begin by considering the function  $F(x)$ , defined by equation (B3), which can be expressed as follows:

$$F(x) = \ln \frac{\cosh 2\alpha b - \cos \alpha x}{\cosh 2\alpha b - \cos \alpha r} + \ln \frac{1 - \cos \alpha r}{1 - \cos \alpha x} \quad (B8)$$

The first term on the right of equation (B8) can be expressed as follows:

$$\begin{aligned} \ln \frac{\cosh 2\alpha b - \cos \alpha x}{\cosh 2\alpha b - \cos \alpha r} &= \ln \frac{1 - \frac{\cos \alpha x}{\cosh 2\alpha b}}{1 - \frac{\cos \alpha r}{\cosh 2\alpha b}} \\ &\approx \ln \left[ \left( 1 - \frac{\cos \alpha x}{\cosh 2\alpha b} \right) \left( 1 + \frac{\cos \alpha r}{\cosh 2\alpha b} \right) \right] \\ &\approx \ln \left( 1 + \frac{\cos \alpha r - \cos \alpha x}{\cosh 2\alpha b} \right) \end{aligned} \quad (B9)$$

or

$$\ln \frac{\cosh 2\alpha b - \cos \alpha x}{\cosh 2\alpha b - \cos \alpha r} \approx \frac{\cos \alpha r}{\cosh 2\alpha b} - \frac{\cos \alpha x}{\cosh 2\alpha b} \quad (B10)$$

The first term on the right of equation (B8) has been reduced to a two-term Fourier cosine series by making successive first-order expansions of terms of the form  $1 \pm \nu$ , where  $\nu \ll 1$ .

APPENDIX - Continued

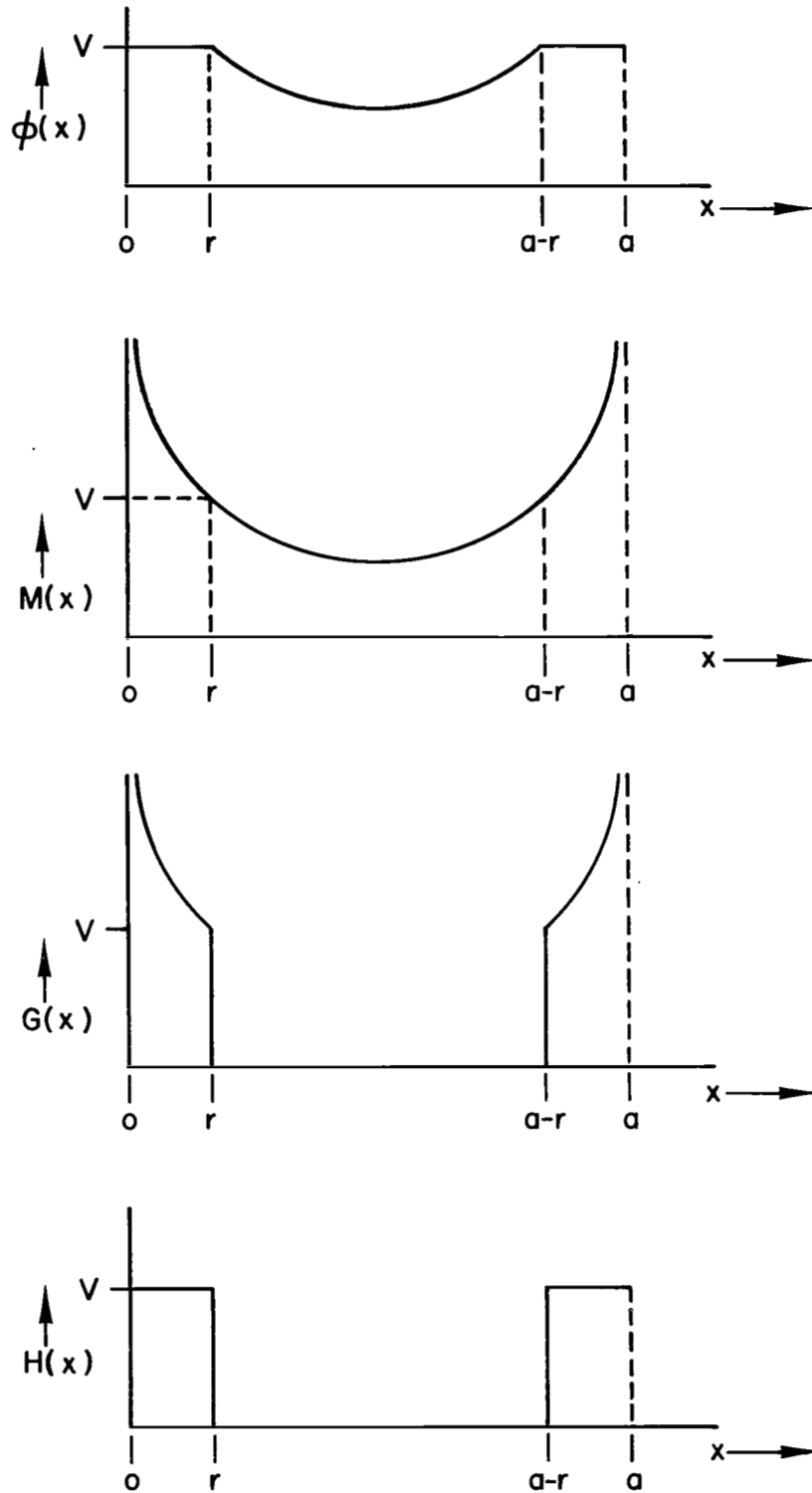


Figure B1.- Illustration of combination of  $M(x)$ ,  $G(x)$ , and  $H(x)$  to form  $\phi(x)$  according to the formula  $\phi(x) = M(x) - G(x) + H(x)$ .

APPENDIX B – Continued

The second term on the right of equation (B8) can be expressed as follows:

$$\ln \frac{1 - \cos \alpha r}{1 - \cos \alpha x} = \frac{1}{2} \ln \left( \frac{1 - \cos \alpha r}{1 - \cos \alpha x} \right)^2 = \frac{1}{2} \ln(1 - \cos \alpha r)^2 - \frac{1}{2} \ln(\cos \alpha x - 1)^2 \quad (\text{B11})$$

The following equality comes from page 358 of reference 13:

$$-\frac{1}{4} \left\{ \ln 4 + \ln [(\cos \alpha x) - 1]^2 \right\} = \sum_{n=1}^{\infty} \frac{\cos n\alpha x}{n} \quad (\text{B12})$$

and can be expressed as

$$\ln [(\cos \alpha x) - 1]^2 = -4 \sum_{n=1}^{\infty} \frac{\cos n\alpha x}{n} - \ln 4$$

or

$$\frac{1}{2} \ln(1 - \cos \alpha x)^2 = -2 \sum_{n=1}^{\infty} \frac{\cos n\alpha x}{n} - \ln 2 \quad (\text{B13})$$

Equation (B13) is inserted into equation (B11) to obtain

$$\ln \frac{1 - \cos \alpha r}{1 - \cos \alpha x} = 2 \sum_{n=1}^{\infty} \frac{\cos n\alpha x}{n} + \ln 2 + \frac{1}{2} \ln(1 - \cos \alpha r)^2 \quad (\text{B14})$$

Equations (B14) and (B10) are inserted into (B8) to yield, after some algebraic manipulation,

$$F(x) = \frac{\cos \alpha r}{\cosh 2\alpha b} + \ln \left( 4 \sin^2 \frac{\alpha r}{2} \right) - \frac{\cos \alpha x}{\cosh 2\alpha b} + 2 \sum_{n=1}^{\infty} \frac{\cos n\alpha x}{n} \quad (\text{B15})$$

This function is then used in equation (B4) to form the Fourier series representation of  $M(x)$ :

$$M(x) = V + VT \left[ \frac{\cos \alpha r}{\cosh 2\alpha b} + \ln \left( 4 \sin^2 \frac{\alpha r}{2} \right) \right] - \frac{VT \cos \alpha x}{\cosh 2\alpha b} + 2VT \sum_{n=1}^{\infty} \frac{\cos n\alpha x}{n} \quad (\text{B16})$$

The next function to be analyzed is  $G(x)$ , defined in equation (B5). In the region where  $G(x)$  is nonzero,

APPENDIX B – Continued

$$\cosh 2\alpha b - \cos \alpha x \approx \cosh 2\alpha b - \cos \alpha r$$

Therefore  $F(x)$ , defined in equation (B3), can be expressed to a good approximation as

$$F(x) \approx \ln \frac{1 - \cos \alpha r}{1 - \cos \alpha x} \quad [0 < x < r, (a-r) < x < a] \quad (B17)$$

From equations (B17), (B4), and (B5),

$$G(x) \approx \begin{cases} V + VT \ln \frac{1 - \cos \alpha r}{1 - \cos \alpha x} & (0 < x < r) \\ 0 & [r < x < (a-r)] \\ V + VT \ln \frac{1 - \cos \alpha r}{1 - \cos \alpha x} & [(a-r) < x < a] \end{cases} \quad (B18)$$

The general form of the cosine expansion of  $G(x)$  is:

$$G(x) = \frac{a_0}{2} + \sum_{n=1}^{\infty} a_n \cos n\alpha x$$

where

$$\left. \begin{aligned} a_0 &= \frac{2}{a} \int_0^a G(x) dx \\ a_n &= \frac{2}{a} \int_0^a G(x) \cos n\alpha x dx \end{aligned} \right\} \quad (B19)$$

First  $a_0$  will be evaluated. Figure B1 shows that  $G(x)$  is a symmetric function. It is symmetric about  $a/2$ ; that is,  $G\left(\frac{a}{2} + x\right) = G\left(\frac{a}{2} - x\right)$  for  $0 < x < a$ . This fact can be verified by direct substitution into equation (B18).

Since  $G(x) = 0$  for  $r < x < (a - r)$ ,  $a_0$  can be evaluated as follows:

$$a_0 = \frac{2}{a} \int_0^r V + VT \ln \frac{1 - \cos \alpha r}{1 - \cos \alpha x} dx + \frac{2}{a} \int_{a-r}^a V + VT \ln \frac{1 - \cos \alpha r}{1 - \cos \alpha x} dx \quad (B20)$$

APPENDIX B – Continued

Because  $G(x)$  is symmetric about  $a/2$ , equation (B20) can be written as

$$a_0 = \frac{4}{a} \int_0^r V + VT \ln \frac{1 - \cos \alpha r}{1 - \cos \alpha x} dx \quad (\text{B21})$$

Since  $\alpha = \frac{2\pi}{a}$  and because of the thin-wire approximation  $r \ll a$ , equation (B21) can be put into a more tractable form. Since

$$\cos \theta \approx 1 - \frac{\theta^2}{2}$$

for small  $\theta$ ,

$$\ln \frac{1 - \cos \alpha r}{1 - \cos \alpha x} \approx \ln \left( \frac{\alpha r}{\alpha x} \right)^2 = 2 \ln \frac{r}{x}$$

Thus, equation (B21) becomes:

$$a_0 \approx \frac{4}{a} \int_0^r \left( V + 2VT \ln \frac{r}{x} \right) dx$$

or

$$a_0 = \frac{4Vr}{a} (1 + 2T) \quad (\text{B22})$$

Similar arguments apply to the evaluation of  $a_n$  (i.e., symmetric  $G(x)$  and thin-wire approximation). Therefore,

$$a_n = \frac{4}{a} \int_0^r \left( V + 2VT \ln \frac{r}{x} \right) \cos n\alpha x dx \quad (\text{B23})$$

After evaluating this integral, the result is

$$a_n = \frac{4V}{2n\pi} \left[ \sin n\alpha r + 2T \text{Si}(n\alpha r) \right] \quad (\text{B24})$$

where

$$\text{Si}(n\alpha r) \equiv \int_{\mu=0}^{\mu=n\alpha r} \frac{\sin \mu}{\mu} d\mu$$

is the sine integral function, which is tabulated in the literature (see, for example, ref. 14).

APPENDIX B – Concluded

Since equations (B22) and (B24) are the Fourier coefficients of  $G(x)$ , the Fourier series of  $G(x)$  is

$$G(x) = \frac{2Vr}{a}(1 + 2T) = \sum_{n=1}^{\infty} \frac{4V}{2n\pi} [\sin(n\alpha r) + 2T \text{Si}(n\alpha r)] \cos n\alpha x \quad (\text{B25})$$

The final function to be analyzed is  $H(x)$ , defined in equation (B6). For the cosine expansion of  $H(x)$ , the Fourier coefficients are derived in the same way they were derived for  $G(x)$ . They are

$$a_0 = \frac{4Vr}{a}$$

$$a_n = \frac{2V \sin n\alpha r}{n\pi}$$

Therefore,

$$H(x) = \frac{2Vr}{a} + \sum_{n=1}^{\infty} \frac{2V \sin n\alpha r}{n\pi} \cos n\alpha x \quad (\text{B26})$$

The Fourier series of  $M(x)$ ,  $G(x)$ , and  $H(x)$  have now been derived in equations (B16), (B25), and (B26), respectively. When these equations are inserted into equation (B7), the result is a cosine expansion of  $\phi(x,b)$ . Then, after some algebraic manipulation,

$$\begin{aligned} \phi(x,b) = V \left\{ 1 - \frac{4Tr}{a} + T \left[ \frac{\cos \alpha r}{\cosh 2\alpha b} + 2 \ln \left( 2 \sin \frac{\alpha r}{2} \right) \right] \right\} + \left\{ \frac{2VT [\pi - 2 \text{Si}(\alpha r)]}{\pi} \right. \\ \left. - \frac{VT}{\cosh 2\alpha b} \right\} \cos \alpha x + \sum_{n=2}^{\infty} \frac{2VT}{\pi} \frac{\pi - 2 \text{Si}(n\alpha r)}{n} \cos n\alpha x \quad (\text{B27}) \end{aligned}$$

This series was programed into a computing calculator and plots of  $\phi(x,b)$  as a function of  $x$  were made for a variety of geometric parameters, keeping 15 terms of the series. These plots coincided with plots of  $\phi(x,b)$  as it is expressed in equation (B1), verifying that equation (B27) is indeed the Fourier cosine expansion of equation (B1).

## APPENDIX C

### DERIVATION OF GRID-PLATE CAPACITANCE FROM THE GRID-PLATE POTENTIAL DISTRIBUTION

Equation (2), repeated here for convenience, relates the capacitance of an arbitrary condenser to the potential distribution inside that condenser:

$$C = \frac{\epsilon}{V^2} \int_{\tau} (\nabla\phi)^2 d\tau$$

For a parallel grid-plate condenser, the potential distribution is described by equation (29):

$$\begin{aligned} \phi(x,y,z) = V & \left\{ 1 - \frac{4Tr}{a} + T \left[ \frac{\cos \alpha r}{\cosh 2\alpha b} + 2 \ln \left( 2 \sin \frac{\alpha r}{2} \right) \right] \right\} \frac{z}{b} + \frac{VT}{\sinh \alpha b} \left\{ \frac{2[\pi - 2 \text{Si}(\alpha r)]}{\pi} \right. \\ & \left. - \frac{1}{\cosh 2\alpha b} \right\} \sinh \alpha z (\cos \alpha x + \cos \alpha y) \\ & + \frac{2VT}{\pi} \sum_{n=2}^{\infty} \frac{\pi - 2 \text{Si}(n\alpha r)}{n} \frac{\sinh n\alpha z}{\sinh n\alpha b} (\cos n\alpha x + \cos n\alpha y) \end{aligned}$$

It is necessary to insert equation (29) into (2) to find the capacitance of the grid-plate condenser.

Since  $\phi(x,y,z)$  is an infinite series of the form

$$\phi = \phi_0 + \phi_1 + \sum_{n=2}^{\infty} \phi_n \tag{C1}$$

then

$$\nabla\phi = \nabla\phi_0 + \nabla\phi_1 + \sum_{n=2}^{\infty} \nabla\phi_n$$

and

$$\begin{aligned} (\nabla\phi)^2 = (\nabla\phi_0)^2 + (\nabla\phi_1)^2 + \left( \sum_{n=2}^{\infty} \nabla\phi_n \right)^2 + 2\nabla\phi_0 \cdot \nabla\phi_1 + 2\nabla\phi_0 \cdot \sum_{n=2}^{\infty} \nabla\phi_n + 2\nabla\phi_1 \cdot \sum_{n=2}^{\infty} \nabla\phi_n \end{aligned} \tag{C2}$$

APPENDIX C – Continued

The third term on the right side of equation (C2) can be more clearly expressed as the sum of two series:

$$\left( \sum_{n=2}^{\infty} \nabla \phi_n \right)^2 = \sum_{n=2}^{\infty} (\nabla \phi_n)^2 + \sum_{\substack{n \ m \\ n \neq m}} \nabla \phi_n \nabla \phi_m \quad (\text{C3})$$

Equation (C2) thus becomes

$$\begin{aligned} (\nabla \phi)^2 = & (\nabla \phi_0)^2 + (\nabla \phi_1)^2 + \sum_{n=2}^{\infty} (\nabla \phi_n)^2 + 2\nabla \phi_0 \cdot \nabla \phi_1 + 2\nabla \phi_0 \cdot \sum_{n=2}^{\infty} \nabla \phi_n + 2\nabla \phi_1 \cdot \sum_{n=2}^{\infty} \nabla \phi_n \\ & + \sum_{\substack{n \ m \\ n \neq m}} \nabla \phi_n \nabla \phi_m \end{aligned} \quad (\text{C4})$$

Since each of the terms on the right side of equation (C4) is composed of products of complete functions, if the grid is assumed to be composed of an integral number of meshes (a condition which insures the conservation of integral periodicity), the integrals of the fourth, fifth, sixth, and seventh terms on the right side of equation (C1) are zero by orthogonality. What remains is

$$\int_{\tau} (\nabla \phi)^2 d\tau = \int_{\tau} \sum_{n=0}^{\infty} (\nabla \phi_n)^2 d\tau \quad (\text{C5})$$

where

$$\phi_0 = \frac{A_0 V z}{b} \quad (\text{C6a})$$

$$\phi_n = A_n V \sinh n\alpha z (\cos n\alpha x + \cos n\alpha y) \quad (\text{C6b})$$

with

$$A_0 = 1 - \frac{4rT}{a} + T \left[ \frac{\cos \alpha r}{\cosh 2\alpha b} + 2 \ln \left( 2 \sin \frac{\alpha r}{2} \right) \right]$$

$$A_1 = \frac{T}{\sinh \alpha b} \left\{ \frac{2[\pi - 2 \text{Si}(\alpha r)]}{\pi} - \frac{1}{\cosh 2\alpha b} \right\}$$

APPENDIX C – Continued

$$A_n = \frac{2T}{\sinh n\alpha b} \frac{\pi - 2 \operatorname{Si}(n\alpha r)}{n\pi} \quad (n \geq 2)$$

$$\alpha = \frac{2\pi}{a}$$

$$T = \frac{1}{4 \ln \left[ \frac{1}{r} \left( \sqrt{b^2 - r^2} + b \right) \right]}$$

From equations (C6),

$$(\nabla\phi_0)^2 = \left( \frac{A_0 V}{b} \right)^2 \quad (C7a)$$

and

$$(\nabla\phi_n)^2 = (n\alpha V D_n \sinh n\alpha z)^2 (\sin^2 n\alpha x + \sin^2 n\alpha y) + (n\alpha V D_n \cosh n\alpha z)^2 (\cos n\alpha x + \cos n\alpha y)^2 \quad (C7b)$$

The plate and grid are assumed to have a length  $L$  and a width  $W$  and to be spaced a distance  $b$  apart. Therefore  $L$ ,  $W$ , and  $b$  represent the limits of integration in the  $x$ -,  $y$ -, and  $z$ -direction, respectively. Equation (C5) becomes

$$\int_{\tau} (\nabla\phi)^2 d\tau = \sum_{n=0}^{\infty} \int_{z=0}^{b=z} \int_{y=0}^{W=y} \int_{x=0}^{L=x} (\nabla\phi_n)^2 dx dy dz \quad (C8)$$

Equations (C7a) and (C7b) must be integrated:

$$\int_{z=0}^{b=z} \int_{y=0}^{W=y} \int_{x=0}^{L=x} (\nabla\phi_0)^2 dx dy dz = \frac{V^2 A_0^2 LW}{b} \quad (C9a)$$

$$\int_{z=0}^{b=z} \int_{y=0}^{W=y} \int_{x=0}^{L=x} (\nabla\phi_n)^2 dx dy dz = \frac{V^2 LW n\alpha D_n^2 \sinh 2n\alpha b}{2} \quad (C9b)$$

Combining equations (C8) and (C9) yields

$$\int_{\tau} (\nabla\phi)^2 d\tau = V^2 LW \left( \frac{A_0^2}{b} + \sum_{n=1}^{\infty} \frac{n\alpha A_n^2 \sinh 2n\alpha b}{2} \right) \quad (C10)$$

APPENDIX C – Concluded

Equation (C10) is inserted into equation (2) to obtain

$$C = \frac{LW\epsilon}{b} \left( A_0^2 + \sum_{n=1}^{\infty} A_n^2 \frac{n\alpha b \sinh 2n\alpha b}{2} \right) \quad (C11)$$

The term outside the parentheses is the well-known formula for the capacitance of a parallel-plate condenser. The expression inside the parentheses represents the change in capacitance when one of the plates is replaced by a square-mesh grid of wires of radius  $r$ , separated by an axis-to-axis distance  $a$ . The series converges very rapidly and only a small number of terms need be retained to insure a high degree of accuracy.

## REFERENCES

1. Whiddington, R.: The Ultra-Micrometer; an Application of the Thermionic Valve to the Measurement of Very Small Distances. *Phil. Mag.*, ser. 6, vol. 40, no. 239, Nov. 1920, pp. 634-639.
2. Sucksmith, W.: The Application of the Ultra-Micrometer to the Measurement of Small Increments of Temperature. *Phil. Mag.*, ser. 6, vol. 43, no. 253, Jan. 1922, pp. 223-226.
3. Whiddington, R.; and Hare, A.: Note on the Ultramicrometer Used as a Differential Micromanometer. *Phil. Mag.*, ser. 6, vol. 46, no. 274, Oct. 1923, pp. 607-608.
4. Whiddington, R.; and Long, F. A.: Note on the Application of the Ultramicrometer to the Microbalance. *Phil. Mag.*, ser. 6, vol. 49, no. 289, Jan. 1925, pp. 113-121.
5. Foldvari, Tibor L.; and Lion, Kurt S.: Capacitive Transducers. *Instrum. Contr. Syst.*, vol. 37, no. 11, Nov. 1964, pp. 77-85.
6. Cotterell, K.: Capacitance Probes for Measurement of Tube Diameter. *Non-Destruct. Test.*, vol. 1, no. 4, May 1968, pp. 245-248.
7. Skalski, C. A.: Capacitance Distance Transducer. *Proc. IEEE*, vol. 56, no. 1, Jan. 1968, pp. 111-112.
8. Jackson, John David: *Classical Electrodynamics*. John Wiley & Sons, Inc., c.1962.
9. Sokolnikoff, Ivan S.; and Sokolnikoff, Elizabeth S.: *Higher Mathematics for Engineers and Physicists*. Second ed., McGraw-Hill Book Co., Inc., 1941.
10. Cairo, Laurent; and Kahan, Théo (G. D. Sims, transl.): *Variational Techniques in Electromagnetism*. Blackie & Son, Ltd., 1965.
11. Ryshik, I. M.; and Gradstein, I. S.: *Summen-, Produkt- und Integral-Tafeln (Tables of Series, Products, and Integrals)*. Second rev. ed., Veb Deutscher Verlag der Wissenschaften (Berlin), 1963.
12. Harrison, D.: Calculation of Capacitance - Use of Geometrical Inversion. *Electron. Radio Eng.*, vol. 34, no. 1, Jan. 1957, pp. 21-25.
13. Bromwich, T. J. I'a.: *An Introduction to the Theory of Infinite Series*. Rev. second ed., Macmillan and Co., Ltd., 1942.
14. Selby, Samuel M., ed.; and Girling, Brian, contrib. ed.: *Standard Mathematical Tables*. Fourteenth ed., Chem. Rubber Co., c.1965.